Lab on a Chip

Cite this: *Lab Chip*, 2011, **11**, 1054

www.rsc.org/loc

PAPER

Nanocavity electrode array for recording from electrogenic cells

Boris Hofmann,[ab] Enno Kätelhön,[ab] Manuel Schottdorf,[ab] Andreas Offenhäusser[ab] and Bernhard Wolfrum*[ab]

Received 10th November 2010, Accepted 10th January 2011
DOI: 10.1039/c0lc00582g

We present a new nanocavity device for highly localized on-chip recordings of action potentials from individual cells in a network. Microelectrode recordings have become the method of choice for recording extracellular action potentials from high density cultures or slices. Nevertheless, interfacing individual cells of a network with high resolution still remains challenging due to an insufficient coupling of the signal to small electrodes, exhibiting diameters below 10 μm. We show that this problem can be overcome by a new type of sensor that features an electrode, which is accessed *via* a small aperture and a nanosized cavity. Thus, the properties of large electrodes are combined with a high local resolution and a good seal resistance at the interface. Fabrication of the device can be performed with state-of-the-art clean room technology and sacrificial layer etching allowing integration of the devices into sensor arrays. We demonstrate the capability of such an array by recording the propagation of action potentials in a network of cardiomyocyte-like cells.

Introduction

Analysis of electrical cellular communication is of great interest for many research fields. Investigations range from cardiac activity[1–3] and pharmacology[4,5] over retina analysis[6] to the synaptic plasticity between individual neurons.[7,8] All these fields are currently pushed by the improvement of extracellular recording devices. Electrical recordings are routinely carried out using microelectrode arrays (MEAs)[4,9–11] or field-effect transistors,[12] which locally probe the extracellular potential at the cell–sensor interface. During the last decades the performance of recording devices has improved and opened many new sites of research. While recording of tissue, slices, or confluent cultures can easily be performed using commercially available devices, interfacing of individual cells still remains challenging. The local resolution of standard microelectrodes is limited by the high interface impedance occurring upon electrode miniaturization. A high impedance causes additional noise and therefore lowers the signal-to-noise ratio of extracellular measurements. For this reason electrode sizes in commercial chip-based electrode arrays are usually well above 10 μm and therefore bigger than the size of an individual cell. Thus, recorded signals cannot be attributed to a specific cell in a network, which reduces the specificity of the information gained from the experimental data. Several attempts for overcoming this problem exist. Nanowire based recording devices offer great opportunities in cell recording,[13] even on a subcellular[14] or intracellular level.[15,16] Furthermore the combination of CMOS techniques with microelectrodes enables on-chip amplification at a high sensor density.[17–20] However, these devices are neither commercially available nor easy to fabricate and limited to research groups equipped with advanced CMOS fabrication technology or e-beam lithography. Surface modifications of planar MEAs with nanoflakes,[21] carbon nanotubes,[8,22–24] gold spines,[25,26] nanorods[27] or nanowires[28,29] have been successfully tested for impedance reduction of electrodes, but they often lack the reproducibility in fabrication, homogeneity, and stability for standard applications. The planar patch clamp technique[30,31] allows to probe individual cells but cannot reach the required sensor density for the analysis of network activity and additionally requires a backside fluidic approach. Here, we demonstrate a simple, yet effective, method for the fabrication of a sensor array suited for extracellular recording of action potentials with single-cell resolution. In our device a liquid filled nanocavity over the electrode is accessed *via* a small microaperture. This approach provides the advantage of a low impedance electrode with a high surface area in combination with a small recording aperture for monitoring individual cells.

[a]*PGI-8/ICS-8, Forschungszentrum Jülich GmbH, Jülich, Germany*
[b]*JARA—Fundamentals of Future Information Technology, 52425 Jülich, Germany. E-mail: b.wolfrum@fz-juelich.de*

Experimental

Nanocavity array fabrication

The chips were fabricated on a 4-inch silicon wafer that was oxidized under wet conditions to grow 1 μm of SiO_2. A fabrication scheme is shown in Fig. 1. First, the electrodes, feed lines, and bond pads were patterned in a double layer resist (LOR3B/nLOF2020, MicroChem Corp., USA, and MicroChemicals GmbH, Germany, respectively). The metal was deposited using electron beam evaporation of 10 nm Ti, 150 nm Au, and 5 nm Cr followed by a lift-off in acetone and MIF326 (MicroChemicals). In a second lithography step, a thin chromium layer of 70 nm was patterned on top of the electrodes. The chromium served as

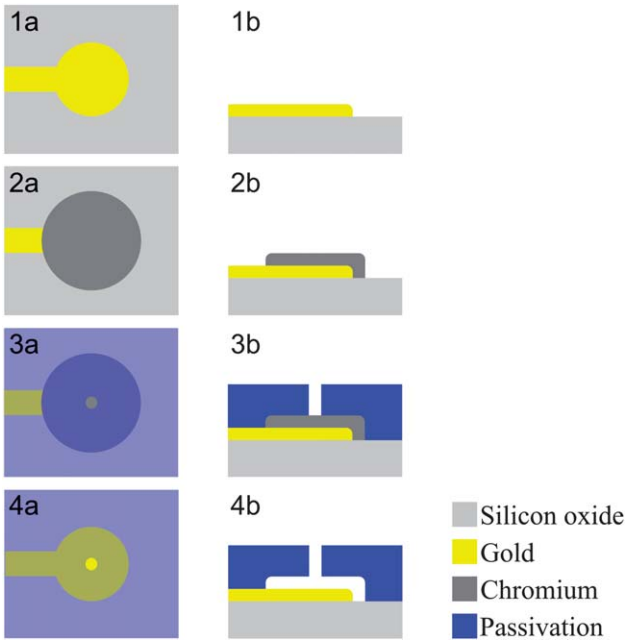

Fig. 1 Fabrication scheme of a single nanocavity sensor. Left and right columns show the top and side view of the sensor, respectively. In a first step the electrodes are patterned (1) followed by the deposition of a sacrificial chromium layer (2). The device is then insulated with a PECVD silicon nitride/silicon oxide layer and an aperture is etched by RIE (3). In a final step the chromium layer is removed using wet chemical etching to form the actual nanocavity. The fabricated chip features are an array of 5 × 6 nanocavity sensors.

a sacrificial layer and defined the later geometry of the nanocavities.[32,33] Afterwards, the whole structure was passivated using a stack of 400 nm silicon nitride and 400 nm silicon oxide deposited by plasma enhanced chemical vapor deposition (SENTECH Instruments GmbH). The bond pads were opened and small apertures of 3 or 5 μm in the center of each electrode were introduced into the passivation layer by reactive ion (CHF_3/CF_4/O_2) etching. Finally the sacrificial layer was removed by wet chemical etching (chromium etch, Merck) to reveal the electrode surfaces inside the nanocavities.

Measurement setup

We used a custom, 64-channel amplifier system equipped with high-impedance operational amplifiers (preamplifier gain 10.22), coupled to a main amplifier (gain 100) providing an overall gain of 1022. Data were sampled simultaneously across all channels at 10 kHz per channel using the MED64 Conductor 3.1 software (Alpha MED Sciences, Japan). An extracellular Ag/AgCl electrode, set to ground potential, served as a reference electrode. A more detailed description of the data acquisition has been published previously.[34]

Cell culture

The HL-1 cell line (Louisiana State University Health Science Center, New Orleans, LA, USA) was derived from AT-1 cells (mouse cardiomyocyte tumor). It represents a hybrid between embryonic and adult myocytes.[35] The HL-1 cardiac muscle cells generate spontaneous APs and subsequently contract after the cells reach confluency. Cells were cultured in T25 flasks at 37 °C and 5% CO_2 in Claycomb Medium with 10% FBS, 100 μg ml^{-1} penicillin–streptomycin, 0.1 mM norepinephrine and 2 mM L-glutamine in a humidified chamber. The cells were seeded onto the chips as described by Law *et al.*,[1] after they reached confluency. Briefly, cells were trypsinized using 0.05% trypsin/EDTA. Trypsinization was stopped by adding the medium followed by centrifugation (5 min, 500*g*). The supernatant was removed and the pellet was resuspended in 1 ml of culture medium. After counting the cells, approximately 3000 cells per mm^2 were plated in 50 μl of medium on the nanocavity chip, previously coated with gelatin fibronectin. After 4 hours of adhesion, chips were topped up with 500 μl of medium. The medium was changed daily until cells reached confluency and measurements were performed, usually 3–4 days after seeding.

Results and discussion

The final electrode array consists of 5 times 6 electrodes as shown in Fig. 2. The height of the cavity is in the range of 50 nm while the width matches the metal electrode. The aperture can be designed in a way to match the desired recording properties.

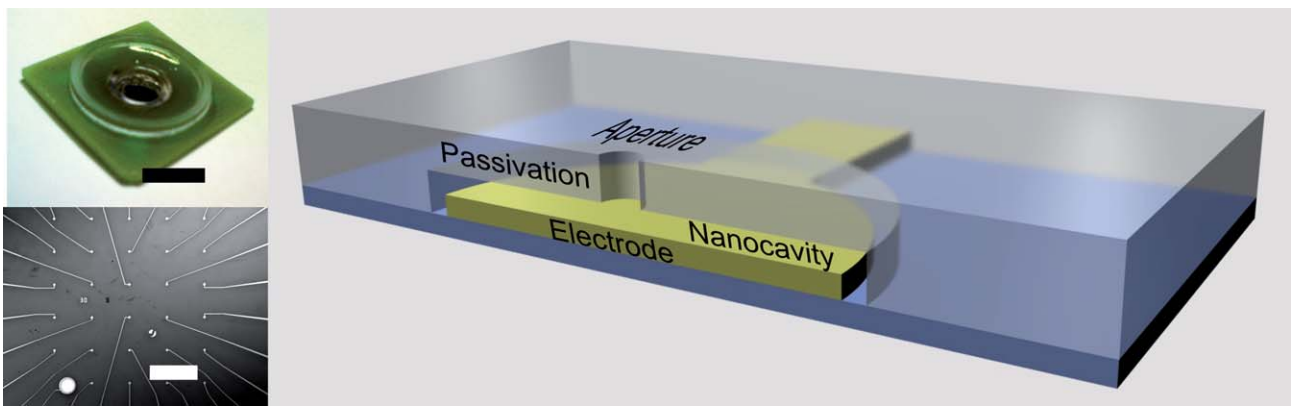

Fig. 2 Final device and schematic of a nanocavity electrode. Top left: final chip bonded to printed circuit board and encapsulated for use in cell culture. Bottom left: microscopic image of the chip showing the layout of the nanocavity electrodes. 5 × 6 sensors are arranged with a pitch of 350 μm in vertical and 400 μm in horizontal directions. Scale bars correspond to 1 cm and 500 μm, respectively. Right: schematic drawing of a cross-section through a single nanocavity sensor, fabricated as described in Fig. 1.

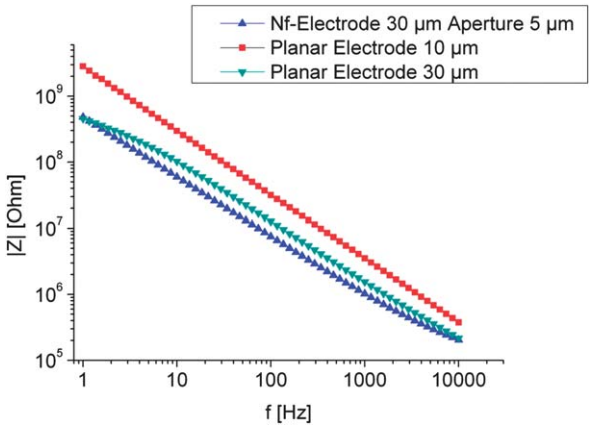

Fig. 3 Impedance spectra of planar electrodes with a diameter of 10 and 30 µm and a 30 µm nanocavity electrode.

Single cell recordings for example should be performed with an aperture diameter that is smaller than the addressed cell to ensure sufficient spatial resolution and a good seal between cell and electrode. A schematic cross-section of a single electrode with the nanocavity is given in Fig. 2.

The quality of the cell–electrode coupling is determined by several key factors as described by Rutten.[36] Most important, the cell should tightly seal the electrode from the bulk with a high junction resistance. This ensures that upon cell activity a measurable potential change is generated at the sensor interface. Further, the electrode impedance has to be sufficiently small to allow for good signal-to-noise ratios during extracellular recording.[37] Finally, the parasitic capacitance of the chip and amplifier system should be small to avoid signal attenuation due to leakage currents. The electrode impedance is in direct correlation with the inverse of the electrode surface. Thus, on the one hand, the demand of low impedances imposes a limit on the minimal size of the recording electrode. On the other hand, single-cell resolution requires that the electrode does not exceed the size of the investigated cell. In our approach, we combine the interfacial properties of a larger microelectrode with a tunable recording-aperture size of several hundred nanometres to micrometres, thus providing a large electrode with a small recording spot. Increasing the electrode surface area *via* a nanofluidic cavity does not change the spot that determines the spatial resolution of the recording. Nevertheless, the effect of the increased electrode area on the impedance is evident. Fig. 3 shows an AC impedance scan between 1 Hz and 10 kHz performed on a planar 30 µm electrode and on a nanocavity electrode with a diameter of 30 µm and an access aperture of 5 µm. As expected, the nanocavity electrode shows almost the same impedance as the planar electrode even though it is only accessed *via* the small aperture.

We investigated the behaviour of the nanocavity electrode under cell culture conditions. To this end, the chips were cultured with HL-1 cells, a cardiomyocyte-like cell line that grows confluent layers coupled *via* gap junctions. The cells autonomously generate action potentials that subsequently spread over the cell layer. The cells were seeded and after 3–4 days in the culture the chips were ready to be measured. In Fig. 4 one can see an SEM picture of a focused ion beam (FIB) cut through a not yet confluent cell layer sitting on top of a nanocavity device. In the center of the cut we see the aperture with the attached cell. The picture depicts the size of the cavity and the bridge the passivation layer forms over the cavity. A close-up view of the aperture is given in the inset. The cleft between the electrode and the passivation can be seen. Furthermore, the cell nicely covers the aperture and grows into the cavity effectively sealing the electrode.

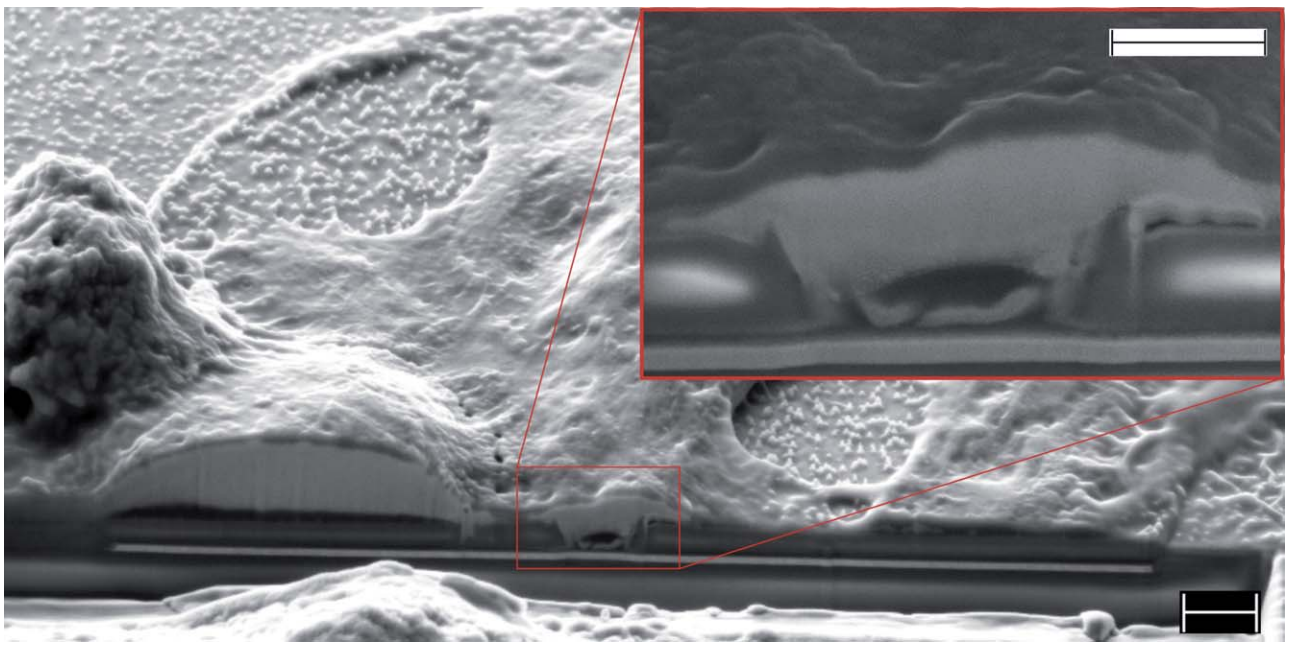

Fig. 4 SEM image of a FIB cut of HL-1 cells growing on a nanocavity electrode as depicted in Fig. 2. The inset shows the aperture region of the electrode. Scale bars correspond to 2 µm and 1 µm, respectively.

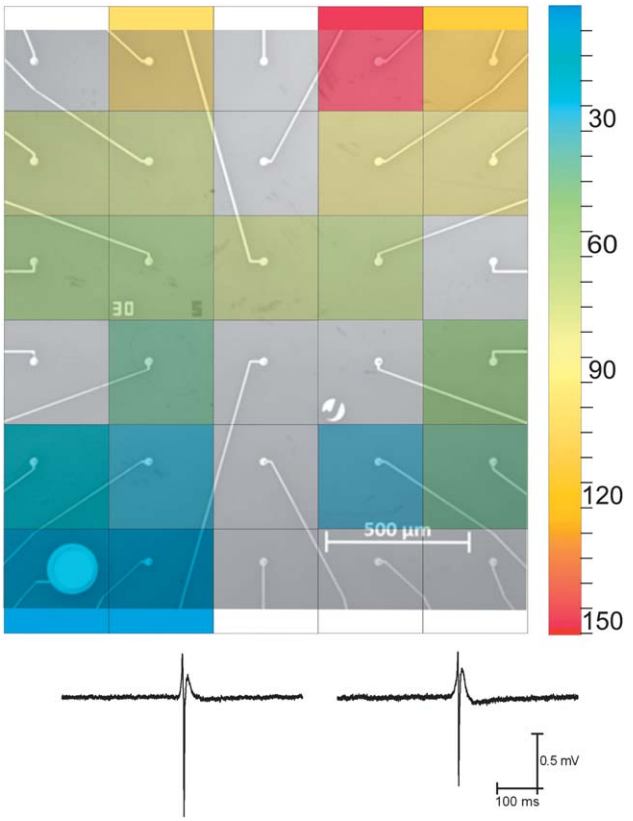

Fig. 5 Propagation of action potentials recorded with a nanocavity electrode array. *Top*: microscopic image of a nanocavity electrode array. The coloured squares depict the time stamp of the detected action potential in ms for each sensor. The signal approaches from the bottom left and propagates to the top right corner. *Bottom*: individual extracellular recordings of two nanocavity electrodes.

Recordings performed with a confluent layer of HL-1 cells are shown in Fig. 5. The image reveals the positions of each electrode on the chip. The propagation of the action potential over the cell layer is depicted in a color code, corresponding to the time delay between the first measured action potential and subsequent action potentials at different locations. Below the image in Fig. 5, examples of individual action potentials are shown. The recorded signals have peak to peak amplitudes of up to 1.5 mV_{p-p} with a typical noise level of 9.5 ± 0.5 μV_{RMS}. Compared to 30 µm planar gold chips the recording performance was not altered significantly in terms of noise, but an increase of the peak to peak AP amplitudes was visible (data not shown). We attribute the increased peak potential to a better seal (increased junction resistance) induced by the small aperture. Furthermore, the recording location can be exactly determined and correlated to an individual cell, due to the small sensor aperture.

Conclusion

We have presented a new type of sensor array based on a nanocavity electrode design that is addressed *via* a microaperture. There are obvious advantages of this new concept for extracellular microelectrode array recordings. The liquid filled nanocavity effectively reduces the impedance of the sensor, which is dominated by the size of the electrode–electrolyte interface. In contrast, the spatial resolution of the sensor is not affected and is only determined by the aperture connecting to the nanocavity. Thus, a high resolution provided by a small aperture allows the exact assignment of individual cells to the respective recording electrodes. Furthermore, single cells are able to completely cover the apertures leading to an increased seal resistance and consequently a better cell–electrode coupling. The strong coupling in combination with a low electrode impedance now enables the analysis of individual cells, that are integrated into dense clusters. Finally, the nanocavity devices can be fabricated in a reliable and controllable way *via* standard optical lithography.

Acknowledgements

The authors thank Marko Banzet for clean room support, Norbert Wolters and Ralph Otto for building the electronic amplifiers and Daniela Eßer for preparation of the FIB-cuts. The work was funded by the Young Investigators Program of the Helmholtz Association.

References

1 J. K. Y. Law, C. K. Yeung, B. Hofmann, S. Ingebrandt, J. A. Rudd, A. Offenhäusser and M. Chan, *Physiol. Meas.*, 2009, **30**, 155–167.
2 J. Hescheler, M. Halbach, U. Egert, Z. Lu, H. Bohlen, B. Fleischmann and M. Reppel, *J. Electrocardiol.*, 2004, **37**, 110–116.
3 B. Hofmann, V. Maybeck, S. Eick, S. Meffert, S. Ingebrandt, P. Wood, E. Bamberg and A. Offenhäusser, *Lab Chip*, 2010, **10**, 2588–2596.
4 A. Stett, U. Egert, E. Guenther, F. Hofmann, T. Meyer, W. Nisch and H. Haemmerle, *Anal. Bioanal. Chem.*, 2003, **377**, 486–495.
5 A. F. M. Johnstone, G. W. Gross, D. G. Weiss, O. H.-U. Schroeder, A. Gramowski and T. J. Shafer, *NeuroToxicology*, 2010, **31**, 331–350.
6 K. Homma, F. Osakada, Y. Hirami, Z.-B. Jin, M. Mandai and M. Takahashi, *J. Neurosci. Res.*, 2009, **87**, 2175–2182.
7 E.-M. Steidl, E. Neveu, D. Bertrand and B. Buisson, *Brain Res.*, 2006, **1096**, 70–84.
8 M. Shein, A. Greenbaum, T. Gabay, R. Sorkin, M. David-Pur, E. Ben-Jacob and Y. Hanein, *Biomed. Microdevices*, 2009, **11**, 495–501.
9 A. Blau, C. Ziegler, M. Heyer, F. Endres, G. Schwitzgebel, T. Matthies, T. Stieglitz, J. U. Meyer and W. Göpel, *Biosens. Bioelectron.*, 1997, **12**, 883–892.
10 J. L. Novak and B. C. Wheeler, *J. Neurosci. Methods*, 1988, **23**, 149–159.
11 Y. Nam, B. C. Wheeler and M. O. Heuschkel, *J. Neurosci. Methods*, 2006, **155**, 296–299.
12 P. Fromherz, *Ann. N. Y. Acad. Sci.*, 2006, **1093**, 143–160.
13 B. P. Timko, T. Cohen-Karni, G. Yu, Q. Qing, B. Tian and C. M. Lieber, *Nano Lett.*, 2009, **9**, 914–918.
14 F. Patolsky, B. P. Timko, G. Yu, Y. Fang, A. B. Greytak, G. Zheng and C. M. Lieber, *Science*, 2006, **313**, 1100–1104.
15 B. Tian, T. Cohen-Karni, Q. Qing, X. Duan, P. Xie and C. M. Lieber, *Science*, 2010, **329**, 830–834.
16 P. Verma and N. A. Melosh, *Appl. Phys. Lett.*, 2010, **97**, 033704.
17 U. Frey, C. D. Sanchez-Bustamante, T. Ugniwenko, F. Heer, J. Sedivy, S. Hafizovic, B. Roscic, M. Fussenegger, A. Blau, U. Egert, and A. Hierlemann, *Conference Proceedings: Annual International Conference of the IEEE Engineering in Medicine and Biology Society*, 2007, pp. 167–170.
18 S. Hafizovic, F. Heer, T. Ugniwenko, U. Frey, A. Blau, C. Ziegler and A. Hierlemann, *J. Neurosci. Methods*, 2007, **164**, 93–106.
19 K. Imfeld, S. Neukom, A. Maccione, Y. Bornat, S. Martinoia, P.-A. Farine, M. Koudelka-Hep and L. Berdondini, *IEEE Trans. Biomed. Eng.*, 2008, **55**, 2064–2073.
20 L. Berdondini, K. Imfeld, A. Maccione, M. Tedesco, S. Neukom, M. Koudelka-Hep and S. Martinoia, *Lab Chip*, 2009, **9**, 2644–2651.

21 J.-H. Kim, G. Kang, Y. Nam and Y.-K. Choi, *Nanotechnology*, 2010, **21**, 85303.
22 T. D. B. Nguyen-Vu, H. Chen, A. M. Cassell, R. Andrews, M. Meyyappan and J. Li, *Small*, 2006, **2**, 89–94.
23 G. Gabriel, R. Gómez, M. Bongard, N. Benito, E. Fernández and R. Villa, *Biosens. Bioelectron.*, 2009, **24**, 1942–1948.
24 E. W. Keefer, B. R. Botterman, M. I. Romero, A. F. Rossi and G. W. Gross, *Nat. Nanotechnol.*, 2008, **3**, 434–439.
25 A. Hai, J. Shappir and M. E. Spira, *Nat. Methods*, 2010, **7**, 200–202.
26 A. Hai, A. Dormann, J. Shappir, S. Yitzchaik, C. Bartic, G. Borghs, J. P. M. Langedijk and M. E. Spira, *J. R. Soc. Interface*, 2009, **6**, 1153–1165.
27 H. B. Zhou, G. Li, X. N. Sun, Z. H. Zhu, Q. H. Jin, J. L. Zhao and Q. S. Ren, *J. Microelectromech. Syst.*, 2009, **18**, 88–96.
28 A. Vlad, M. Mátéfi-Tempfli, S. Faniel, N. Reckinger, B. Olbrechts, A. Crahay, V. Bayot, L. Piraux, S. Melinte and S. Mátéfi-Tempfli, *Small*, 2008, **4**, 557–560.
29 H. Yoon, D. C. Deshpande, V. Ramachandran and V. K. Varadan, *Nanotechnology*, 2008, **19**, 025304.
30 N. Fertig, R. H. Blick and J. C. Behrends, *Biophys. J.*, 2002, **82**, 3056–3062.
31 N. Fertig, M. Klau, M. George, R. H. Blick and J. C. Behrends, *Appl. Phys. Lett.*, 2002, **81**, 4865.
32 E. Kätelhön, B. Hofmann, S. G. Lemay, M. A. G. Zevenbergen, A. Offenhäusser and B. Wolfrum, *Anal. Chem.*, 2010, **82**, 8502–8509.
33 B. Wolfrum, M. Zevenbergen and S. Lemay, *Anal. Chem.*, 2008, **80**, 972–977.
34 H. Ecken, S. Ingebrandt, M. Krause, D. Richter, M. Harac and A. Offenhäusser, *Electrochim. Acta*, 2003, **48**, 3355–3362.
35 W. C. Claycomb, N. A. Lanson, B. S. Stallworth, D. B. Egeland, J. B. Delcarpio, A. Bahinski and N. J. Izzo, *Proc. Natl. Acad. Sci. U. S. A.*, 1998, **95**, 2979–2984.
36 W. L. C. Rutten, *Annu. Rev. Biomed. Eng.*, 2002, **4**, 407–452.
37 W. Franks, I. Schenker, P. Schmutz and A. Hierlemann, *IEEE Trans. Biomed. Eng.*, 2005, **52**, 1295–1302.

